Electronic Supplementary Material (ESI) for Physical Chemistry Chemical Physics.
This journal is © the Owner Societies 2016

Molecular Design of Light-Harvesting Photosensitizers: Effect of Varied Linker Conjugation on Interfacial Electron Transfer

Jianbing Jiang†, John R. Swierk†, Svante Hedström, Adam J. Matula, Robert H. Crabtree*, Victor S. Batista**, Charles A. Schmuttenmaer*and Gary W. Brudvig*
Department of Chemistry and Energy Sciences Institute, Yale University, New Haven, Connecticut, 06520, USA

Table of Contents

Experimental Details

Methods. All chemicals and solvents were commercially available and used as obtained, without further purification. ^{1}H NMR spectra were recorded at 400 MHz, and ^{13}C NMR spectra were recorded at 100 MHz. Chemical shifts are reported as ppm from the internal reference tetramethylsilane (TMS). High-resolution mass spectrometry (HRMS) was performed on a Q-TOF LC−MS with API by direct injection of a methanolic solution at ~0.5 mg/mL concentration. Steady-state absorption spectra were recorded on a Varian Cary 50 Bio UV-visible spectrophotometer. Fluorescence spectra were recorded on a Shimadzu RF-5301pc spectrofluorophotometer. Compounds **1,**[1] **2,**[2] **3,**[3] **4,**[4] **5,**[5] and **6**[6] were prepared according to reported procedures.

Characterization. All compounds were characterized by ^{1}H NMR and HR-MS. The Ruthenium complexes (esters) were characterized by steady-state absorption and fluorescence spectrometry. ^{13}C NMR spectra were also recorded for compounds **Amide1** and **Stilb**, but not for others due to insufficient solubility.

Scheme S1: Synthetic Scheme for Ru1, Ru2, and Ru3.

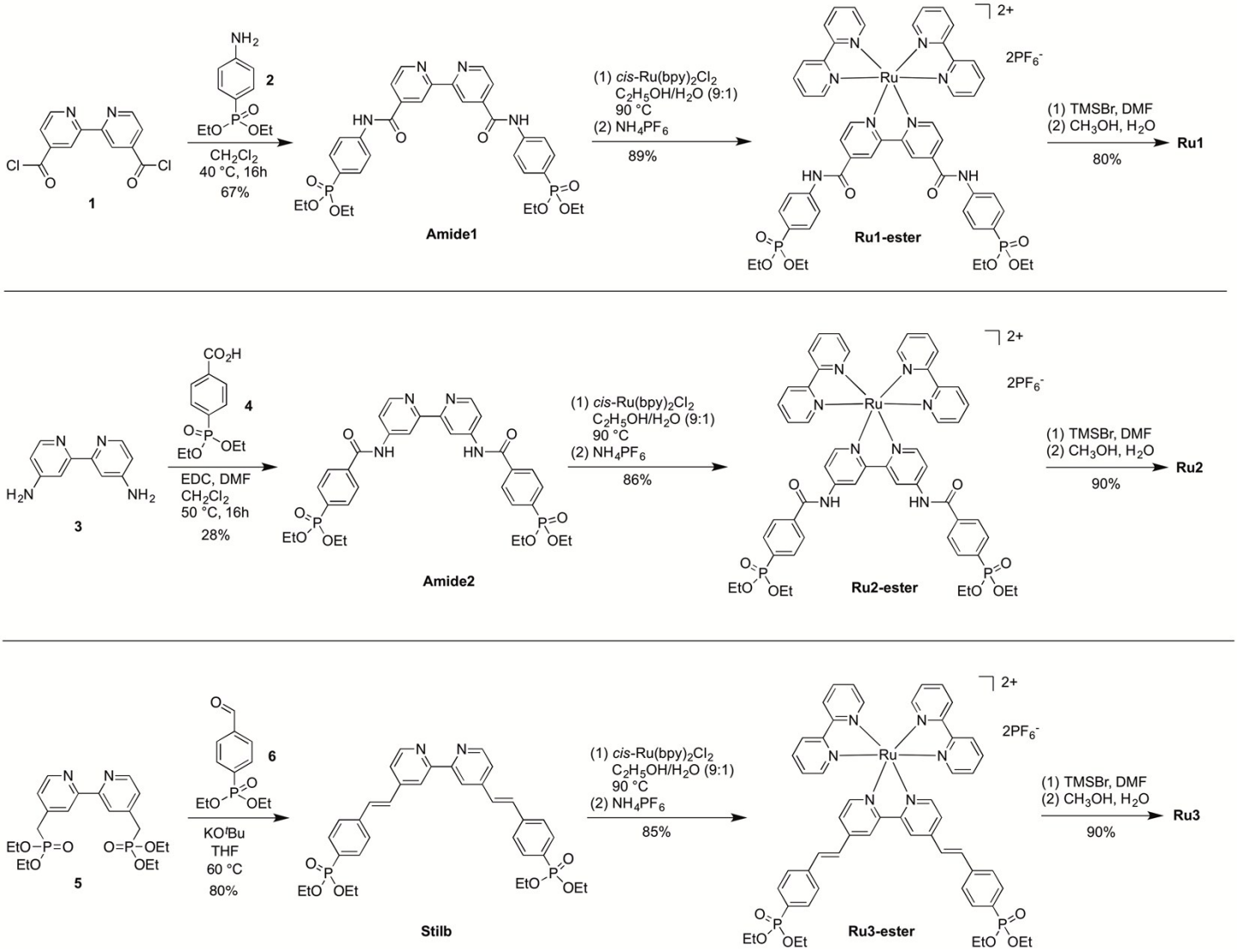

Amide1. A solution of **2** (963 mg, 4.20 mmol) in CH_2Cl_2 (5.0 mL) was added to a solution of 4,4'-di(chlorocarbonyl)-2,2'-bipyridine **1** (556 mg, 2.0 mmol) in CH_2Cl_2 (5.0 mL). A pink precipitate formed immediately after addition. The mixture was heated to 40 °C and stirred under nitrogen for 16 h. The suspension was centrifuged, and the supernatant was discarded. The crude residue was washed successively with 1 N HCl, water and CH_2Cl_2. The product was dried to afford the title compound as a pink solid. (892 mg, 67%). ^{1}H NMR ($CDCl_3$), 1.23 (t, J = 7.0 Hz, 12H), 3.93–4.07 (m, 8H), 7.72 (d, J = 12 Hz, 2H), 7.74 (d, J = 12 Hz, 2H), 7.99 (m, 6H), 8.91 (s, 2H), 8.96 (d, J = 4.0 Hz, 2H), 10.97 (s, 2H); ^{13}C NMR (CD_3OD + $CDCl_3$), 19.8, 66.4, 123.2, 124.2, 126.1, 136.5, 146.4, 147.5, 154.0, 160.1, 169.2; ESI-MS obsd 667.1946, calcd 667.2081 [$(M + H)^+$, M = $C_{32}H_{36}N_4O_8P_2$].

Ru1-ester. A solution of **Amide1** (333 mg, 0.5 mmol) and *cis*-[$Ru(bpy)_2Cl_2$] (260 mg, 0.5 mmol) in a solvent mixture of C_2H_5OH and H_2O (30 mL, 9:1, v/v) was stirred at 90 °C under nitrogen for 20 h. The solvents were removed by rotary evaporation. The dark residue was dissolved in a minimum amount of water and CH_3CN (~2.0 mL, 1:1, v/v) and loaded to a LH20 column. Pure CH_3CN was first used to remove the unreacted *cis*-[$Ru(bpy)_2Cl_2$], and then changed to 7% of CH_3OH in CH_3CN. The dark orange band was collected. The solvents were removed by rotary evaporation. The residue was dissolved in a minimum amount of water (~2.0 mL), and then a saturated solution of NH_4PF_6 (~20 mL) was added. The suspension was centrifuged, and the supernatant was discarded to afford a dark orange solid, which was washed twice with water. The solid was dried under high vacuum to afford a dark orange powder. (610 mg, 89%). ^{1}H NMR (DMSO-d_6), 1.23 (t, J = 8.0 Hz, 12H), 3.93–4.07 (m, 8H), 7.55 (m, 4H), 7.72–7.80 (m, 8H), 7.91–7.99 (m, 8H), 8.17–8.23 (m, 4H), 8.87 (d, J = 8.0 Hz, 4H), 9.39 (s, 2H); ESI-MS obsd 540.1193, calcd 540.1208 (M^{2+}, M = $C_{52}H_{52}N_8O_8P_2Ru$).

Ru1. To a solution of **Ru1-ester** (63 mg, 0.051 mmol) in DMF (2.57 mL) was added TMSBr (81.4 μL, 0.617 mmol, 12 eq) under nitrogen. The solution was stirred under nitrogen at 60 °C in the dark for 18 h. DMF and excess TMSBr were removed under high vacuum at °C. To the orange residue was added a mixture of solvents (8.0 mL CH_3OH + 0.5 mL H_2O) and the mixture was stirred at room temperature for 3 h. Diethyl ether was added to the reaction mixture, the suspension was centrifuged, and the supernatant was discarded to afford an orange solid. The solid was dried under high vacuum to afford a dark orange powder (46.4 mg, 80%). ^{1}H NMR (DMSO-d_6), 7.55 (q, J = 8.0 Hz, 4H), 7.66–7.86 (m, 12H), 7.55–7.59 (m, 4H), 8.88 (d, J = 8.0 Hz, 4H), 9.43 (s, 2H), 10.93 (s, 4H); ESI-MS obsd 484.0622, calcd 484.0582 (M^{2+}, M = $C_{44}H_{36}N_8O_8P_2Ru$).

Amide2. A sample of phosphanobenzoic acid **4** (1.032 g, 4.0 mmol) and EDC (1.15 g, 6.0 mmol) in CH_2Cl_2 (4.0 mL) was stirred at room temperature under nitrogen for 40 min (Solution A). In a separate vial, diaminodipyridine **3** (372 mg, 2.0 mmol) was dissolved in DMF (3 mL) and stirred for 3 min (Solution B). Solution B was then transferred via pipette to solution A. The resulting mixture was stirred under nitrogen at 50 °C for 16 h. To the crude mixture was added water, and the precipitate was isolated and washed successively with 1 N HCl, saturated $NaHCO_3$ and hexanes. The grey solid was dried to afford the title compound (747 mg, 28%). ^{1}H NMR ($CDCl_3$), 1.24 (t, J = 7.0 Hz, 12H), 4.00–4.12 (m, 8H), 7.88 (d, J = 12.0 Hz, 2H), 7.90 (d, J = 12.0 Hz, 2H), 7.94 (dd, $J1$ = 8.0 Hz, $J2$ = 3.0 Hz, 2H), 8.62 (d, J = 8.0 Hz, 2H), 8.85 (d, J = 4.0 Hz, 2H), 10.90 (s, 2H); ESI-MS obsd 667.2052, calcd 667.2081 [$(M + H)^+$, M = $C_{32}H_{37}N_4O_8P_2$].

Ru2-ester. A solution of **Amide2** (11.1 mg, 0.017 mmol) and *cis*-[$Ru(bpy)_2Cl_2$] (8.7 mg, 0.017 mmol) in a solvent mixture of ethanol and water (1.0 mL, 9:1, v/v) was stirred at 90 °C under nitrogen for 12 h. The solvents were removed by rotary evaporation. The crude dark residue was dissolved in a minimum amount of water and CH_3CN (~1.0 mL, 1:1, v/v) and loaded to a LH20 column. Pure CH_3CN was first used to remove the reacted *cis*-[$Ru(bpy)_2Cl_2$], and then changed to 7% of methanol in CH_3CN. The dark orange band was collected. The solvents were removed by rotary evaporation. The residue was dissolved in a minimum amount of water (~1.0 mL), and then a saturated solution of NH_4PF_6 (~10 mL) was added. The precipitate was centrifuged, and the supernatant was discarded to afford a dark orange solid, which was washed twice with water. The solid was dried under high vacuum to afford a dark orange powder (20 mg, 86%). ^{1}H NMR (DMSO-d_6), 1.24 (t, J =

8.0 Hz, 12H), 4.00–4.10 (m, 8H), 7.48–7.56 (m, 4H), 7.65 (d, *J* = 8.0 Hz, 2H), 7.71 (d, *J* = 8.0 Hz, 2H), 7.82–7.95 (m, 8H), 8.08–8.18 (m, 8H), 8.83 (d, *J* = 8.0 Hz, 2H), 9.13 (s, 2H); ESI-MS obsd 540.1217, calcd 540.1208 (M^{2+}, M = $C_{52}H_{52}N_8O_8P_2Ru$).

Ru2. To a solution of **Ru2-ester** (25 mg, 0.018 mmol) in DMF (0.91 mL) was added TMSBr (28.9 μL, 0.219 mmol, 12 eq) under nitrogen. The solution was stirred under nitrogen at 60 °C in the dark for 18 h. DMF and excess TMSBr were removed under high vacuum at 60 °C. To the orange residue was added a mixture of solvents (4.0 mL CH_3OH + 0.5 mL H_2O), and the mixture was stirred at room temperature for 6 h. Diethyl ether was added to the reaction mixture, the suspension was centrifuged, and the supernatant was discarded to afford an orange solid. The solid was dried under high vacuum to afford a dark orange powder (46.4 mg, 80%). ^{1}H NMR (DMSO-d_6), 7.49–7.56 (m, 4H), 7.65 (d, *J* = 8.0 Hz, 2H), 7.72 (d, *J* = 4.0 Hz, 2H), 7.83–7.89 (m, 8H), 8.03–8.05 (m, 4H), 8.12–8.18 (m, 4H), 8.83 (d, *J* = 8.0 Hz, 2H), 9.14 (s, 2H), 11.31 (s, 4H); ESI-MS obsd 484.0602, calcd 484.0582 (M^{2+}, M = $C_{44}H_{36}N_8O_8P_2Ru$).

Stilb. To a solution of phosphanomethyldipyridine **5** (182 mg, 0.4 mmol) in THF (2 mL) was added KO^{t}Bu (180 mg, 1.6 mmol), and the resulting suspension was stirred under nitrogen for 10 min. Another solution of phosphanobenzaldehyde **4** (290 mg, 1.2 mmol) in THF (2 mL) was transferred to the former solution, and the resulting mixture was stirred under nitrogen for 16 h. Hexanes were added to the reaction mixture, and the precipitate was isolated and washed with water. The solid was dried to afford the title compound as a grey powder (202 mg, 80%). ^{1}H NMR (CD_3OD), 1.34 (t, *J* = 8.0 Hz, 12H), 4.07–4.20 (m, 8H), 7.46 (d, *J* = 16.0 Hz, 2H), 7.65 (d, *J* = 16.0 Hz, 2H), 7.66 (dd, *J1* = 6.0 Hz, *J2* = 2.0 Hz, 2H), 7.79–7.85 (m, 8H), 8.53 (s, 2H), 8.67 (d, *J* = 8.0 Hz, 2H); ^{13}C NMR (CD_3OD + $CDCl_3$), 16.3, 62.6, 118.8, 121.6, 127.1, 128.8, 132.4, 145.6, 149.7, 156.5; ESI-MS obsd 633.2295, calcd 633.2278 [$(M + H)^+$, M = $C_{34}H_{38}N_2O_6P_2$].

Ru3-ester. A solution of **Stilb** (78.1 mg, 0.123 mmol) and *cis*-[$Ru(bpy)_2Cl_2$] (64.2 mg, 0.123 mmol) in a solvent mixture of C_2H_5OH and H_2O (7.4 mL, 9:1, v/v) was stirred at 95 °C under nitrogen for 20 h. The solvents were removed by rotary evaporation. The crude dark residue was dissolved in a minimum amount of water and CH_3CN (~2.0 mL, 1:1, v/v) and loaded to a LH20 column. Pure CH_3CN was first used to remove the reacted *cis*-[Ru(bpy)2Cl2], then changed to 7% of methanol in CH_3CN. The dark orange band was collected. The solvents were removed by rotary evaporation. The residue was dissolved in a minimum amount of water (~2.0 mL), and then a saturated solution of NH_4PF_6 (~15 mL) was added. The precipitate was centrifuged, and the supernatant was discarded to afford a dark orange solid, which was washed twice with water. The solid was dried under high vacuum to afford a dark orange powder (141 mg, 85%). ^{1}H NMR (CD_3OD), 1.33 (t, *J* = 8.0 Hz, 12H), 4.08–4.17 (m, 8H), 7.46–7.53 (m, 8H), 7.60 (d, *J* = 8.0 Hz, 4H), 7.71–7.83 (m, 16H), 7.93 (d, *J* = 8.0 Hz, 2H), 8.09–8.14 (m, 4H), 8.69 (d, *J* = 8.0 Hz, 4H), 8.96 (s, 2H); ESI-MS obsd 523.1368, calcd 523.1306 (M^{2+}, M = $C_{54}H_{54}N_6O_6P_2Ru$).

Ru3. To a solution of **Ru3-ester** (75 mg, 0.055 mmol) in DMF (2.76 mL) was added TMSBr (87.5 μL, 0.663 mmol, 12 eq) under nitrogen. The solution was stirred under nitrogen at 60 °C in the dark for 12 h. DMF and excess TMSBr were removed under high vacuum at 60 °C. To the orange residue was added a mixture of solvents (4.0 mL CH_3OH + 0.5 mL H_2O), and the mixture was stirred at room temperature for 5 h. Diethyl ether was added to the reaction mixture, the suspension was centrifuged, and the supernatant was discarded to afford an orange solid. The solid was dried under high vacuum to afford a dark orange powder (50.3 mg, 82%). ^{1}H NMR (DMSO-d_6), 7.44–7.90 (m, 22H), 8.14 (t, *J* = 8.0 Hz, 4H), 8.79 (d, *J* = 8.0 Hz, 4H); ESI-MS obsd 467.0668, calcd 467.0680 (M^{2+}, M = $C_{46}H_{38}N_6O_6P_2Ru$).

Sample Preparation. TiO_2 films for transient absorption measurements were prepared on TEC15 fluorine-doped tin oxide (FTO) glass (Hartford Glass Co.). An organic TiO_2 paste (Solaronix Ti-Nanoxide T/SP) was doctor-bladed onto the FTO glass using a single layer of Scotch tape as a spacer layer to give a nominal thickness of 1.2 μm and then then dried at 80 °C for 10 min. After drying, the films were then sintered

in a box furnace at 470 °C for 30 min. The films were sensitized for 16 h in a 0.1 mM solution of dye dissolved in 5:3 0.1M $HClO_4$:DMSO. Transient absorption measurements were made in 0.1 M $HClO_4$.

Samples for THz measurements were prepared on fused quartz substrates as described in detail elsewhere.[7] Briefly, TiO_2 particles were ground with acetic acid, water, and ethanol to form a paste and then ultrasonicated. α-Terpineol and ethyl cellulose were added as binders and the excess ethanol stripped to give a paste. The paste was doctor-bladed onto fused quartz substrates (GM associates) using Scotch tape as a spacer. Each layer was dried at 80 °C before the next layer was added. A total of five layers of TiO_2 were deposited to give a nominal film thickness of 6 μm. The films were sensitized as above and afterwards sealed using a second piece of quartz separated by a 60 μm Surlyn spacer (Solaronix). 0.1 M $HClO_4$ was introduced into the gap between the pieces of quartz via vacuum backfilling.

Transient Absorption Measurements. Nanosecond transient absorption measurements were made using an Edinburgh Instruments LP920 Transient Absorbance Spectrometer. The sample was pumped at 530 nm (2 mJ/pulse) by a Nd:YAG laser (Spectra-Physics INDI-10) passed through an OPO (Spectra-Physics basiScan M). A pulsed 450 W Xe arc lamp was utilized as the probe source. Prior to the sample, the probe was filtered through a 450 nm short pass filter. After the sample, the probe light was passed through a monochromator and into a photomultiplier tube. Changes in absorbance were monitored at 420 nm. Typically 64 shots were averaged and the data were fit to a stretched exponential equation of the form:

$$\Delta A = \Delta A_0 \exp\left[-\left(\frac{t}{\tau}\right)^{\beta}\right] + c \qquad \text{(S1)}$$

where ΔA_0 is the change in absorbance at $t = 0$, τ is the lifetime, β is a stretching parameter ($0 < \beta \leq 1$), and c is an offset at long times. When $\beta = 1$, the equation becomes a single exponential with an offset. The lifetime τ can be used to calculate a rate constant for recombination (k_{obs}) and a weighted lifetime for recombination ($\langle\tau\rangle$) can be calculated from:

$$\langle\tau\rangle = \frac{1}{k_{obs}\beta}\Gamma\left(\frac{1}{\beta}\right) \qquad \text{(S2)}$$

Time-Resolved Terahertz (THz) Spectroscopy (TRTS). The THz spectrometer and technique is described in detail elsewhere.[8-9] Briefly, the 35 fs, 800 nm output of an amplified Ti:sapphire laser (Spectra-Physics) operating a repetition rate of 1 kHz is split into a THz generation beam, a detection beam, and a pump beam. The generation beam is frequency doubled and along with the fundamental harmonic focused in air to generate a plasma.[10,11] The pump beam is likewise frequency doubled to 400 nm and adjusted using a variable neutral density filter to obtain a power of 100 mW (100 μJ/pulse) at a spot size of 10 mm. Before the sample, the laser is passed through a 5 mm diameter aperture. The forward propagating THz pulse generated by the plasma is collected and focused using a series of off-axis paraboloidal mirrors. THz radiation is detected with a ZnTe(110) crystal using free-space electro-optic sampling.[12] The instrument response function was given by a Gaussian function with a full-width at half-maximum of 500 fs and the TRTS scans fit with the following function:

$$\Delta THz = \left\{\Delta THz_0 + \sum_{i=1}^{n} A_i\left[\exp\left(-\frac{t-t_0}{\tau_i}\right)-1\right]\right\} \otimes G(FWHM) \qquad \text{(S3)}$$

where THz_0 is a baseline offset, n is the number of exponential terms used in the fit, A_i is the injection amplitude of a given component, t_0 is the arrival time of the pump pulse, $G(FWHM)$ represents a normalized Gaussian instrument response function, and $\otimes$ is a convolution.

Electrochemistry. The ester versions of Ru1, Ru2, and Ru3 were dissolved in acetonitrile to give a 10 mM solution. Tetrabutylammonium perchlorate was used as a supporting electrolyte (0.1 M). A platinum disk electrode was used as the working electrode and a piece of platinum mesh was used as the counter electrode. A silver wire was utilized as a quasi-reference and the potentials measured relative to ferrocene (0.64 V vs. NHE). The potential was swept at a rate of 10 mV/s.

Dye-Sensitized Solar Cells. DSSCs were fabricated as previously reported.[13] Briefly, a TiO_2 blocking layer was applied to a piece of TEC7 FTO glass (Hartford Glass co.) by immersion in a 40 mM aqueous solution of $TiCl_4$•THF for 30 min at 80 °C before being crystallized at 570 °C for 10 min. An organic TiO_2 paste (Solaronix Ti-Nanoxide T/SP) was doctor-bladed on the substrates using Scotch tape as a spacer layer and cured at 80 °C for 10 min to give a nominal layer thickness of 4 μm. A total of 3 layers were applied to give a TiO_2 thickness of approximately 12 μm. The films were sintered at 470 °C for 30 min and treated again with $TiCl_4$•THF as before being immersed in a 0.1 mM dye solution in 5:3 0.1M $HClO_4$:DMSO for 16 h. Platinum cathodes were prepared by doctor blading an 8 wt% solution of H_2PtCl_6 in ethanol on TEC15 FTO glass and then annealed at 450 °C for 30 min. The anode and cathode were hot-pressed together using a 60 μm Surlyn spacer (Solaronix) and vacuumed backfilled with electrolyte (Iodolyte HI-30).

The photovoltaic characteristics of the solar cells were tested using a solar simulator fitted with an AM-1.5 filter and calibrated using a Si reference diode.

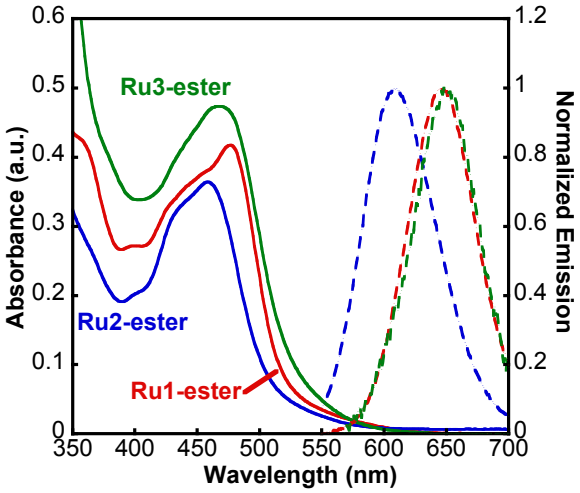

Figure S1: Steady-state absorption spectra (solid line) and emission spectra (dashed lines) of 25 μM **Ru1-ester**, **Ru2-ester**, and **Ru3-ester** in acetonitrile.

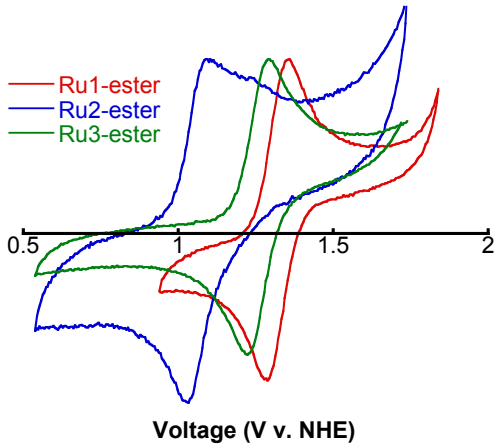

Figure S2: Cyclic voltammagrams of **Ru1-ester**, **Ru2-ester**, and **Ru3-ester** (10 mM) in acetonitrile (0.1 M tetrabutylammonium perchlorate). Pt disk working electrode, Pt mesh counter electrode, Ag wire quasi-referenced to ferrocene (0.64 V vs. NHE).

Table S1: Experimental and Calculated Ground State Potentials for Oxidation vs. NHE and Excited State Potentials

	Experimental			Calculated				
	$Ru^{2+/3+}$	$E_{0\text{-}0}$	$Ru^{3+/2+*}$	$Ru^{2+/3+}$	E_{vert} (S_1)	$Ru^{3+/2+*}$ (S_1)	E_{opt} (T_1)	$Ru^{3+/2+*}$ (T_1)
Ru1	1.32	1.95	-0.63	1.39	2.31	-0.92	1.82	-0.43
Ru2	1.06	2.08	-1.02	1.19	2.55	-1.36	2.05	-0.86
Ru3	1.21	1.93	-0.72	1.20	2.33	-1.13	1.84	-0.64

Electrochemical potentials vs. NHE, $E_{0\text{-}0}$ values are reported in eV

Table S2: Fit parameters for TRTS scans

	A_1	τ_1 (ps)	A_2	τ_2 (ps)	A_3	τ_3 (ps)	THz_o	t_0 (ps)	Scaling Factor
Ru1	0.51	<0.5	0.49	520			0.00	-0.20	0.07
Ru2	0.22	< 0.5	0.23	122	0.55	725	0.00	-0.31	0.32
Ru3	0.18	< 0.5	0.27	63	0.55	501	0.00	-0.23	0.50

Table S3: Operating parameters for DSSCs

	J_{sc} (mA cm^{-2})	V_{oc} (mV)	FF	η (%)
Ru1	0.61 ± 0.02	500 ± 25	0.52 ± 0.07	0.16 ± 0.03
Ru2	0.91 ± 0.03	506 ± 49	0.55 ± 0.11	0.26 ± 0.07
Ru3	0.79 ± 0.12	486 ± 18	0.43 ± 0.03	0.17 ± 0.04
N719	13.85 ± 0.59	637 ± 0	0.52 ± 0.07	5.23 ± 0.10

DFT calculations. All DFT calculations were performed with the Gaussian09 software[14] and the B3LYP exchange–correlation density functional.[15] Optimizations of the S_0 ground state, the T_1 state, and the oxidized state were performed with the SDD basis set and effective core potential on ruthenium and the 6-31G(d) basis set[16] on the remaining atom types. The solvent was represented by a polarizable continuum model of DMSO, using the default settings in Gaussian09. All optimizations were followed by single point calculations with the SDD[Ru]/6-311+G(d,p)[C,H,N,O,P] triple zeta basis set to obtain the state potentials as well as the distributions and energies of the molecular orbitals. Linear-response time-dependent DFT calculations using SDD[Ru]/6-31G(d)[C,H,N,O,P] were used to calculate the $S_0 \rightarrow S_1$ vertical excitation.

Electron injection dynamics. The electron injection from dye to TiO_2 was modeled computationally with a quantum dynamics simulation based on an extended Hückel methodology as previously reported.[17] The binding geometry was first obtained from a system with a CH_3-PO_3^{2-} anchor group chemisorbed in a bidentate fashion to the (101) surface of a $Ti_7O_{27}H_{28}^{2+}$ cluster. This was subjected to a structural optimization using the PBE functional[18] and the Def2SV(P) basis set and density fitting basis set,[19] with all Ti and O atoms frozen in the anatase crystal structure, except the 6 atoms closest to the adsorbate which were allowed to structurally relax together with the methylphosphonate. Using the resulting semi-optimized binding geometry, the 3 dyes in their S_0 geometry were attached to the (101) surface of a $Ti_{128}O_{256}$ slab of anatase in its crystal geometry.

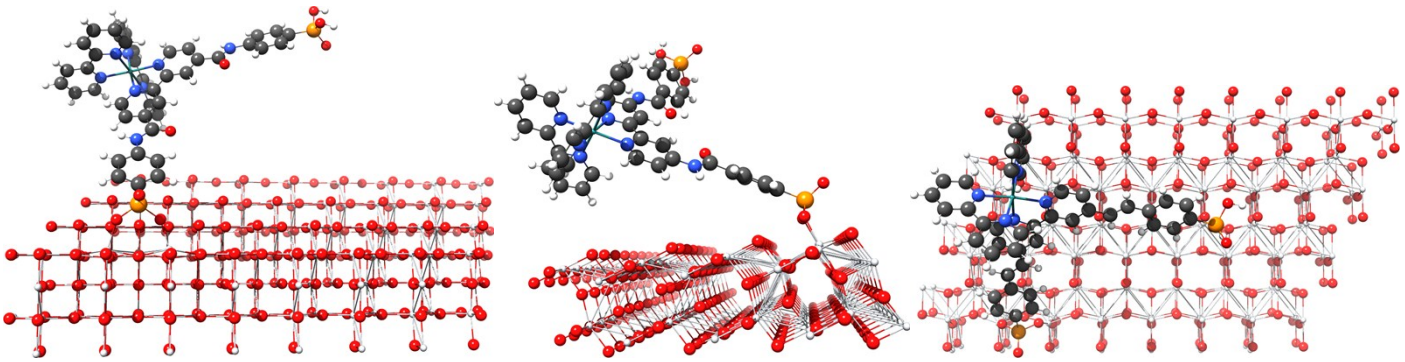

Figure S3. Dye–$Ti_{128}O_{256}$ systems for the injection dynamics calculations. **Ru1** front view, **Ru2** side view, **Ru3** top-view.

The propagation of the wave function of an electron starting in the adsorbate LUMO was then calculated by solving the time-dependent Schrödinger Equation:

$$|\Psi(t)\rangle = \left|\Psi(t)\right\rangle = \Sigma_k \left\langle \phi_k \middle| \Psi(0) e^{-\frac{iE_k t}{\hbar}} \middle| \phi_k \right\rangle$$

$$\left|\Psi(t)\right\rangle = \sum\nolimits_k \left\langle \phi_k \middle| \Psi(0) e^{-\frac{iE_k t}{\hbar}} \middle\rangle \middle| \phi_k \right\rangle \qquad \text{(S4)}$$

Here $|\Psi(0)\rangle$ is the initial wave function with the wave packet in the adsorbate LUMO, the ϕ_k are the molecular orbitals with associated eigenvalues E_k that make up the total wave function, obtained from extended Hückel calculations using the YaEHMOP software.[20] The wave function at time t, $|\Psi(t)\rangle$, was calculated in time steps of 1.0 fs for a total of 1000 fs while monitoring the projection of this wave packet on the TiO_2 basis functions. Exponential dampening absorbing boundary potentials were placed on the sides and bottom of the TiO_2 slab to prevent artificial electron back-transfer events from occurring. These events are known to occur when using PBCs to calculate the energy levels of the TiO_2, and by removing the wave packet from the system when they reach the orbitals of the marked Ti atoms we can prevent them while measuring the overall injection. The norm

of the wave packet decreases when the wave packet density reaches an orbital to which the adsorbing potentials have been applied. To determine the time constant from the dynamics calculations, we fitted an exponential function of time to the decaying wave packet norm:

$$Norm_{WavePacket}(t) = e^{-\frac{t}{\tau}} \quad \text{(S5)}$$

Extended Hückel calculations tend to describe the electronic structure within a single material well but, because the semiempircal energy parameters used in the method are referenced to different vacuum states, when combining two or more types of materials it is important to realign the relevant energy levels. Here, we shifted the adsorbate molecular orbitals towards higher energies as necessary to confer an injection driving force of the same magnitude as observed experimentally.

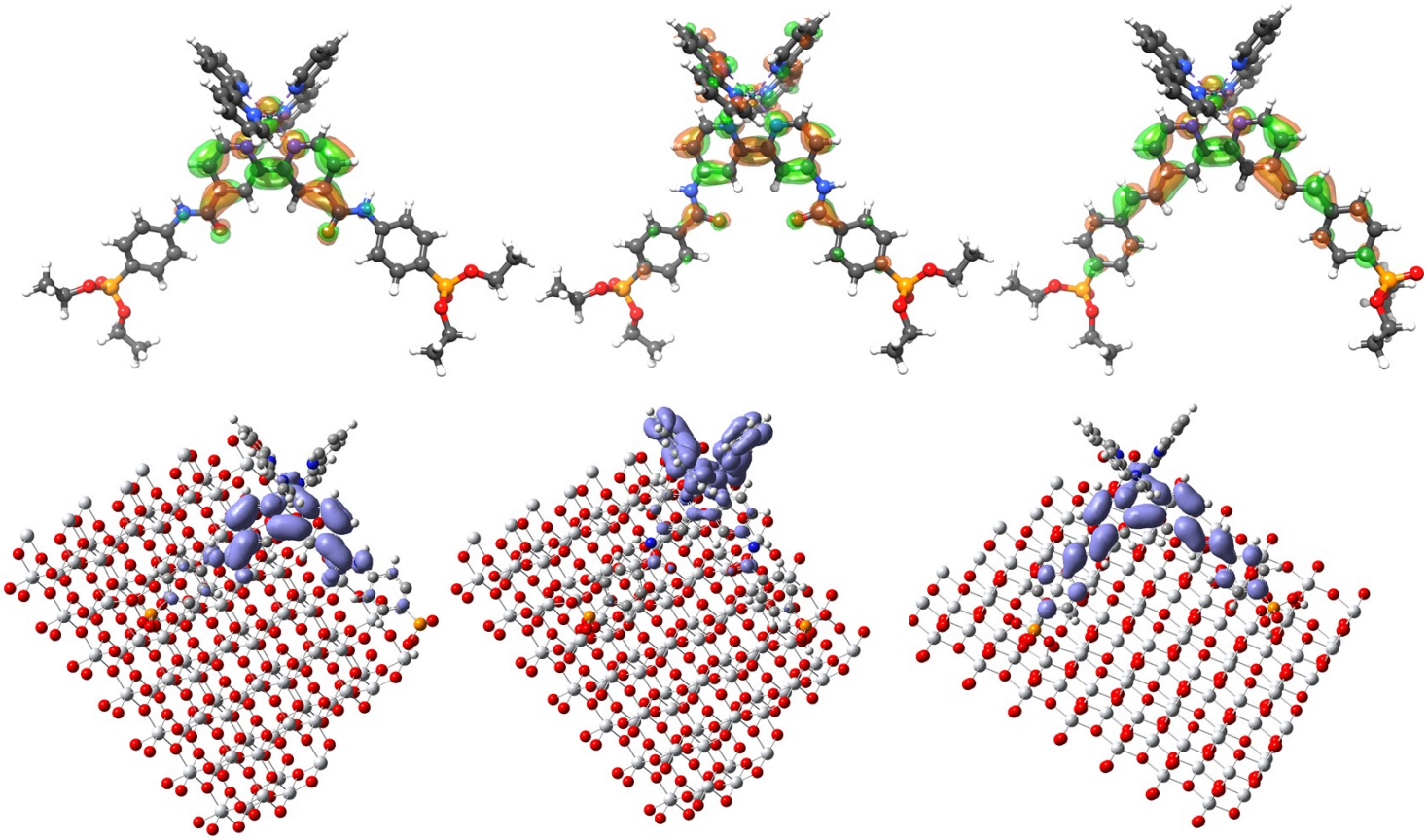

Figure S4. (*Top***)** DFT LUMOs for the ester versions of the dyes. Very good agreement is obtained between the two methods. (*Bottom*) Extended Hückel LUMOs for **Ru**, **Ru2**, and **Ru3** on the $Ti_{128}O_{256}$ slab.

Marcus–type recombination. An attempt was made at estimating the relative recombination rates with a Marcus-type hopping equation, assuming a constant donor state potential, $E_{D,TiO2}$, and a constant coupling, H_{AD}, between the TiO_2 donor state and the dye HOMO acceptor state. This reduces the Marcus prefactor, and yields the following equation for relative rates:

$$\frac{k_1}{k_2} = \sqrt{\frac{\lambda_1}{\lambda_2}} \exp\left(-\frac{(\Delta G_1 + \lambda_1)}{4\lambda_1 k_B T} + \frac{(\Delta G_2 + \lambda_2)}{4\lambda_2 k_B T} \right) \quad , \quad \Delta G = E_{HOMO} - E_{D,TiO_2} \tag{S6}$$

The acceptor HOMO potentials, E_{HOMO}, were obtained from the DFT calculations on the isolated ester versions of the neutral dyes, while the outer-sphere reorganization energies, λ, were obtained by considering the potentials of four states: 1) the fully optimized oxidized dye, 2) the fully optimized neutral dye, 3) the oxidized dye at the geometry and non-equilibrium PCM solvent shell of the neutral dye, and 4) the neutral dye at the geometry and non-equilibrium PCM solvent shell of the oxidized dye. This results in values of λ of 0.633, 0.626, and 0.610 eV for **Ru1**, **Ru2**, and **Ru3**, respectively. However, the correct recombination rate trend between the three dyes is only observed for $E_{D,TiO2} \approx -5.5$ eV vs. vacuum, deeper than physically sensible. It is, therefore, concluded that the recombination occurs not only via direct hopping from TiO_2 to the oxidized dye HOMO, but also through some other mechanism.

References

1. Khatua, S. and Schmittel, M, *Org. Lett.* 2013, **15**, 4422–4425.
2. Nemeth, G, *J. Med. Chem.*, 2014, **57**, 3939–3965.
3. Adams, C. J., Bowen, L. E., Humphrey, M. G., Morrall, J. P. L., Samoc, M. and Yellowlees, L. J., *Dalton Trans.*, 2004, 4130–4138.
4. Beletskaya, I. P., Kabachnik, M. M. and Solntseva, M. D., *Russ. J. Org. Chem.*, 1999, **35**, 71–73.
5. I. Gillaizeau-Gauthier, F. Odobel, M. Alebbi, R. Argazzi, E. Costa, C. A. Bignozzi, P. Qu and G. J. Meyer, *Inorg. Chem.*, 2001, **40**, 6073–6079.
6. Hau, S. K., Cheng, Y.–J., Yip, H.–L., Zhang, Y., Ma, H. Jen, A. K.-Y., *ACS Appl. Mater. Inter.*, 2010, **2**, 1892–1902.
7. J. R. Swierk, N. S. McCool, C. T. Nemes, T. E. Mallouk and C. A. Schmuttenmaer, *J. Phys. Chem. C*, 2016, acs.jpcc.6b00749.
8. M. C. Beard, G. M. Turner and C. A. Schmuttenmaer, *Phys. Rev. B*, 2000, **62**, 15764–15777.
9. C. T. Nemes, C. Koenigsmann and C. A. Schmuttenmaer, *J. Phys. Chem. Lett.*, 2015, **6**, 3257–3262.
10. D. J. Cook and R. M. Hochstrasser, *Opt. Lett.*, 2000, **25**, 1210–1212.
11. T. Bartel, P. Gaal, K. Reimann, M. Woerner and T. Elsaesser, *Opt. Lett.*, 2005, **30**, 2805–2807.
12. Q. Wu and X. C. Zhang, *Appl. Phys. Lett.*, 1995, **67**, 3523–3525.
13. C. Koenigsmann, T. S. Ripolles, B. J. Brennan, C. F. A. Negre, M. Koepf, A. C. Durrell, R. L. Milot, J. A. Torre, R. H. Crabtree, V. S. Batista, G. W. Brudvig, J. Bisquert and C. A. Schmuttenmaer, *Phys Chem Chem Phys*, 2014, **16**, 16629–16641.
14. Gaussian 09, Revision D.01, Frisch, M. J.; Trucks, G. W.; Schlegel, H. B.; Scuseria, G. E.; Robb, M. A.; Cheeseman, J. R.; Scalmani, G.; Barone, V.; Mennucci, B.; Petersson, G. A.; Nakatsuji, H.; Caricato, M.; Li, X.; Hratchian, H. P.; Izmaylov, A. F.; Bloino, J.; Zheng, G.; Sonnenberg, J. L.; Hada, M.; Ehara, M.; Toyota, K.; Fukuda, R.; Hasegawa, J.; Ishida, M.; Nakajima, T.; Honda, Y.; Kitao, O.; Nakai, H.; Vreven, T.; Montgomery, J. A., Jr.; Peralta, J. E.; Ogliaro, F.; Bearpark, M.; Heyd, J. J.; Brothers, E.; Kudin, K. N.; Staroverov, V. N.; Kobayashi, R.; Normand, J.; Raghavachari, K.; Rendell, A.; Burant, J. C.; Iyengar, S. S.; Tomasi, J.; Cossi, M.; Rega, N.; Millam, J. M.; Klene, M.; Knox, J. E.; Cross, J. B.; Bakken, V.; Adamo, C.; Jaramillo, J.; Gomperts, R.; Stratmann, R. E.; Yazyev, O.; Austin, A. J.; Cammi, R.; Pomelli, C.; Ochterski, J. W.; Martin, R. L.; Morokuma, K.; Zakrzewski, V. G.; Voth, G. A.; Salvador, P.; Dannenberg, J. J.; Dapprich, S.; Daniels, A. D.; Farkas, Ö.; Foresman, J. B.; Ortiz, J. V.; Cioslowski, J.; Fox, D. J. Gaussian, Inc., Wallingford CT, 2009.
15. Becke, A.D., *J. Chem. Phys.*, 1993, **98**, 5648-5652.
16. Ditchfield, R. H. W. J., W. J. Hehre, and John A. Pople, *J. Chem Phys.,* 1971, **54**, 724-728.
17. L. G. C. Rego and V. S. Batista, *J. Am. Chem. Soc.*, 2003, **125**, 7989–7997.
18. Perdew, J. P., Burke, K., Ernzerhof, M., *Phys. Rev. Lett.*, 1996, **77**, 3865.
19. Weigend, F., Ahlrichs, R., *Phys. Chem. Chem. Phys.,* 2005, **7**, 3297-3305.
20. G.A.Landrum and W.V.Glassey, **bind** 3.0. in YAeHMOP, overlap.chem.cornell.edu:8080/yaehmop.html